

# Green light emission in silicon through slow-light enhanced third-harmonic generation in photonic-crystal waveguides

B. Corcoran<sup>1</sup>, C. Monat<sup>1\*</sup>, C. Grillet<sup>1</sup>, D. J. Moss<sup>1</sup>, B. J. Eggleton<sup>1</sup>, T. P. White<sup>2</sup>, L. O'Faolain<sup>2</sup> and T. F. Krauss<sup>2</sup>

**Slow light has attracted significant interest recently as a potential solution for optical delay lines and time-domain optical signal processing<sup>1,2</sup>. Perhaps even more significant is the possibility of dramatically enhancing nonlinear optical effects<sup>3,4</sup> due to the spatial compression of optical energy<sup>5-7</sup>. Two-dimensional silicon photonic-crystal waveguides have proven to be a powerful platform for realizing slow light, being compatible with on-chip integration and offering wide-bandwidth and dispersion-free propagation<sup>2</sup>. Here, we report the slow-light enhancement of a nonlinear optical process in a two-dimensional silicon photonic-crystal waveguide. We observe visible third-harmonic-generation at a wavelength of 520 nm with only a few watts of peak power, and demonstrate strong third-harmonic-generation enhancement due to the reduced group velocity of the near-infrared pump signal. This demonstrates yet another unexpected nonlinear function realized in a CMOS-compatible silicon waveguide.**

Although silicon has been the material of choice for the CMOS industry and more recently for integrated photonics, its optical properties—for example, light emission—still provide major challenges. In addition to an indirect bandgap and inversion symmetry, its strong absorption in the visible restricts the potential emission window to wavelengths above  $\sim 800$  nm. Nonlinear optical effects, such as stimulated Raman scattering and third-harmonic generation (THG) offer new ‘tricks’ for light emission<sup>8</sup>, thereby extending the functionality of silicon photonics.

Two-dimensional photonic crystals have recently attracted considerable attention by controlling the propagation of light in unprecedented ways<sup>2,9</sup>. In particular, they can produce slow light<sup>1,2</sup> with the ability to dramatically enhance nonlinear optical phenomena<sup>3,4,7</sup>. However, although nonlinear optical processes have been widely demonstrated in silicon nanowires<sup>2,8,10,11</sup>, corresponding demonstrations in silicon photonic crystals—especially with slow light—have been elusive, only having been reported in the context of the electro-optic coefficient<sup>12</sup>.

Here, we report visible (green light) THG in slow-light silicon photonic-crystal waveguides through end-fire coupling of near-infrared pulses with  $\sim 10$  W peak pump power. This power is five to six orders of magnitude lower than that of earlier THG demonstrations in bulk silicon<sup>13-16</sup> and arises from a combination of extreme mode confinement by the photonic-crystal waveguide, slow-light enhancement and extraction of the visible light through the photonic-crystal lattice.

The generation of third-harmonic light (electric field intensity  $I_{3\omega}$ , frequency  $3\omega$ ) from a fundamental pump beam ( $I_\omega$ ,  $\omega$ )

propagating in a lossless homogeneous waveguide of length  $L$  is given by<sup>17</sup>

$$I_{3\omega} = (3\omega)^2 \left( \frac{2\pi}{nc} \right)^4 I_\omega^3 L^2 (\chi^{(3)})^2 \text{sinc}^2 \left[ \frac{\Delta k(\omega)L}{2} \right] f(A_\omega, A_{3\omega}) \quad (1)$$

where  $\chi^{(3)}$  and  $n$  are the third-order nonlinear susceptibility and refractive index of silicon, respectively,  $\Delta k = k_{3\omega} - 3k_\omega$  is the phase mismatch between the fundamental mode and the third-harmonic wavevectors and  $f(A_\omega, A_{3\omega})$  accounts for the spatial overlap between the two modes. For perfect phase matching ( $\Delta k = 0$ ) and maximum mode overlap ( $f = 1$ ), equation (1) primarily reflects the THG cubic dependence on  $I_\omega$ , which arises from the basic nature of the THG process—that is, converting three  $\omega$  photons into a single  $3\omega$  photon (Fig. 1a). Clearly, then, increasing  $I_\omega$  within the nonlinear material is crucial to enhancing the THG efficiency. This has been achieved in the past by using ultrahigh-Q, small-modal-volume silica microtoroids<sup>18</sup>, although these tend to yield narrow bandwidth and dispersive features. Another approach has been to make use of the high density of states at the band-edge of periodic structures in various materials and geometries, such as Bragg gratings in porous silicon<sup>19,20</sup>, two-dimensional GaN photonic crystals<sup>21</sup> and three-dimensional polystyrene photonic crystals<sup>22</sup>. These schemes generally involve a free-space configuration (reflection or diffraction surface probe experiments) where the lack of optical confinement limits the potential enhancement of  $I_\omega$ , thus requiring megawatt peak pump powers.

Combining optical confinement and dispersion engineering through the use of optimized two-dimensional photonic-crystal waveguides<sup>23-25</sup> is highly promising because  $I_\omega$  is related to the peak power ( $P_\omega$ ) through

$$I_\omega \propto \frac{P_\omega}{A_\omega} \cdot \frac{n_g}{n} \quad (2)$$

where  $A_\omega$  and  $n_g$  are the effective area and group index of the fundamental mode, respectively. Hence, by using the extreme concentration of optical energy afforded by (i) the tight confinement of light within the high-index, sub-micrometre-scale ( $A_\omega \approx 0.4 \mu\text{m}^2$ ) silicon photonic-crystal waveguides and (ii) spatial pulse compression in the slow light ( $v_g = c/40$ ) regime, we significantly reduce the peak pump power required to observe THG to 10 W. In addition, the photonic crystal structure provides a mechanism for light extraction at a wavelength that would otherwise be strongly

<sup>1</sup>CUDOS, Institute for Photonic Optical Sciences (IPOS), School of Physics, University of Sydney, New South Wales 2006, Australia, <sup>2</sup>School of Physics and Astronomy, University of St Andrews, St Andrews, Fife KY16 9SS, UK. \*e-mail: monat@physics.usyd.edu.au

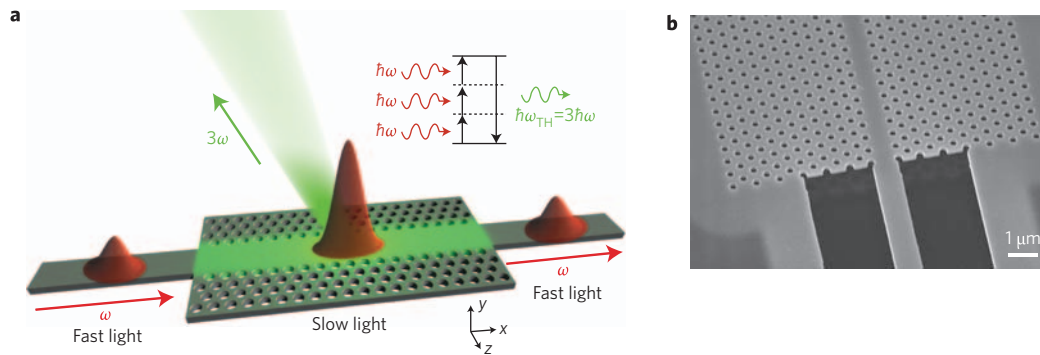


**Figure 1 | Green light emission through third-harmonic generation (THG) in a slow-light photonic-crystal waveguide.** **a**, Schematic of slow-light enhanced THG. The fundamental pulse at frequency  $\omega$  (energy  $\hbar\omega$ ) is spatially compressed in the slow-light photonic-crystal waveguide, increasing the electric field intensity, while the third-harmonic signal, at frequency  $\omega_{\text{TH}} = 3\omega$ , is extracted out-of-plane by the photonic crystal with a specific angle off the vertical direction. **b**, Scanning-electron-microscope (SEM) image of the tapered ridge waveguide connected to the photonic-crystal waveguide etched in a thin silicon membrane. Scale bar,  $1\ \mu\text{m}$ .

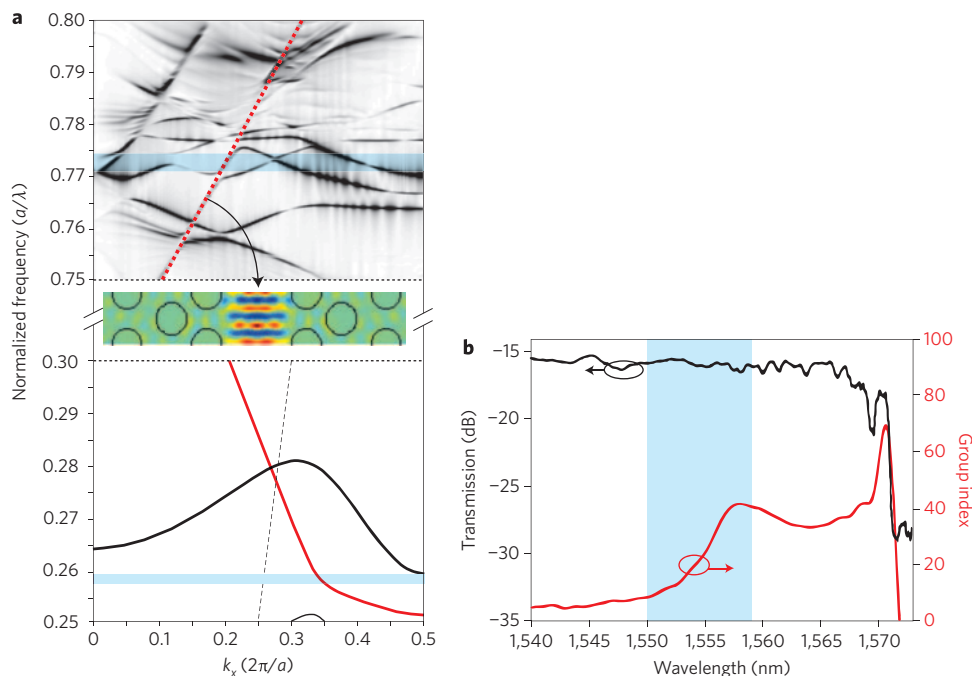


**Figure 2 | Photonic-crystal waveguide dispersion.** **a**, Two-dimensional finite-difference time-domain (FDTD) band structure calculated around  $1,550\ \text{nm}$  ( $a/\lambda = 0.258$ ) and  $520\ \text{nm}$  ( $a/\lambda = 0.77$ ). Only symmetric modes are displayed in the upper frequency window, with the dotted red line highlighting the fundamental refractive-like mode folded back into the first Brillouin zone ( $H_y$  mode profile in the inset) that can sustain the third harmonic. The black dashed line in the lower frequency window represents the light line, with the upper frequency region lying entirely above the light line.  $a$  is the lattice constant of photonic crystal and  $k_x$  is the wavevector in the  $x$ -axis. **b**, Measured transmission and group index of the photonic-crystal waveguide. The blue areas highlight the probed fundamental and third-harmonic spectral regions.

absorbed, thereby opening the spectral emission window of silicon to the visible.

Our device consists of an  $80\text{-}\mu\text{m}$ -long W1 photonic-crystal waveguide in a  $220\text{-nm}$ -thick air-suspended silicon slab, coupled to two tapered ridge waveguides (Fig. 1a,b). Unlike the highly dispersive slow-light mode associated with the band edge of typical photonic-crystal waveguides<sup>26,27</sup>, here the fundamental mode is engineered to display both low group velocity and low dispersion<sup>24</sup> (Fig. 2a,b). Large dispersion typically broadens and distorts short pulses, which tends to compromise the benefits of slow light for nonlinear applications. In our case, however, we focus on the spectral window ( $1,550\text{--}1,559\ \text{nm}$ ) where the measured group velocity of the fundamental mode<sup>28</sup> varies almost linearly by a factor of 4 from  $c/10$  to  $c/40$  (Fig. 2b), enabling us to investigate the effect of group velocity.

When launching a near-infrared  $1.5\text{-ps}$  pulse train ( $4\ \text{MHz}$ ) into the photonic-crystal waveguide, we observe green light emitted from the surface of the chip by eye (Fig. 3a). The emission is directional, being at an angle  $\sim 10^\circ$  from the vertical, in the backward direction, as indicated by the schematic in Fig. 1a. Imaging the emission onto a calibrated linear charge-coupled-device (CCD) camera using a microscope objective with a numerical aperture (NA) of  $0.25$  reveals that it is localized above the photonic-crystal waveguide and decays exponentially along its length (Fig. 3b). The total emitted green power (integrated spatially over the CCD image, Fig. 4) shows a cubic dependence on the coupled pump power of up to  $\sim 65\ \mu\text{W}$ , and is verified to have a wavelength of  $520 \pm 5\ \text{nm}$  using bandpass filters, both of which are expected for a THG process driven by a  $1,560\text{-nm}$  pump. At higher pump powers,

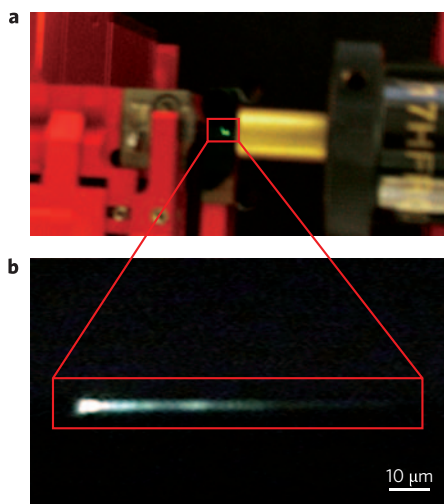


**Figure 3 | Observation of green light.** **a**, Visible green emission from the surface of the chip as seen by eye. **b**, Emission captured by a 0.25 NA microscope objective and imaged onto the CCD camera, with the enclosed box indicating the relative position of the photonic-crystal waveguide; the pump is injected from the left-hand side. Note that the green light emission starts at the entrance of the slow-light photonic-crystal section (after the first 10 photonic-crystal periods stretched to enhance coupling; see Methods) and decays exponentially along the photonic-crystal waveguide length.

a slight saturation occurs in the fundamental power transmission (see Fig. 4) due to two-photon and subsequent free-carrier absorption. We observe a maximum THG output of  $\sim 10$  pW for 80  $\mu\text{W}$  (10 W) average (peak) pump power.

In general, there are a number of effects that can contribute to a variation in the THG efficiency along the waveguide, including group velocity dispersion (GVD) and nonlinear absorption, both of which degrade the fundamental pulse intensity along the photonic-crystal waveguide. It potentially also includes phase matching between the fundamental and third-harmonic modes, although here the extremely short ( $\sim 1$   $\mu\text{m}$ ) absorption length of the third-harmonic light in silicon damps this effect (see Methods). In order to minimize these effects and determine the dependence of the THG efficiency solely on group velocity, we therefore restricted our measurements to a region within 5  $\mu\text{m}$  of the photonic-crystal waveguide entrance, which is much smaller than the dispersion length associated with the GVD, even in the 'fast light' regime (see Methods).

Figure 5a,b shows that the observed THG power displays a clear enhancement for pump wavelengths near 1,557 nm where the group velocity is lowest. Equation (1) predicts a cubic dependence on  $n_g$  of the THG power obtained at a fixed pump power. However, to minimize the nonlinear loss saturation effect discussed above at all wavelengths, we chose instead to plot on Fig. 5c,d the input power density  $P_\omega/A_\omega$  required to produce a constant (and sufficiently low) THG output power ( $\sim 0.2$  pW) as the wavelength (hence group index  $n_g$ ) is varied. By plotting the power density  $P_\omega/A_\omega$  rather than power  $P_\omega$ , we factor out the spectral dependence of  $A_\omega$  and focus on the variation due solely to group index (see Methods). The results show very good agreement with a  $1/n_g$  variation, as expected from equation (2);  $P_\omega/A_\omega \propto I_\omega/n_g$  when considering a constant intensity  $I_\omega$  responsible for a given THG signal. Note that both the trend and the variation in enhancement are well accounted for using only the experimentally measured group velocity dispersion of Fig. 2b. It is clear, then, that any contribution from other effects would cause a discrepancy with experiment, even if (by coincidence) its wavelength dependence happened to be identical to that of  $n_g$ . Hence, we believe these results conclusively demonstrate direct slow-light enhancement of this nonlinear process.

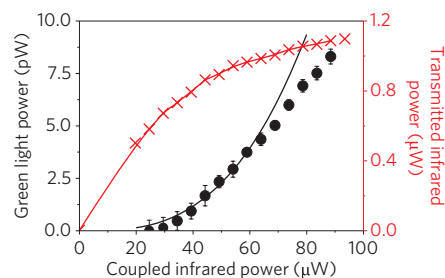


**Figure 4 | Power dependence of the green light emission.** The left axis (black circles) represents the measured visible green power as a function of the average near-infrared power coupled into the waveguide at 1,556.5 nm. The black solid line represents a cubic fit. The error bars are derived from noise estimation on the CCD. The right axis (red crosses) represents the transmitted average near-infrared power through the waveguide structure at 1,556.5 nm.

Our experiments were performed with  $\sim 10$  W peak pump powers, corresponding to a reduction of five to six orders of magnitude compared to previous reports<sup>13–16</sup> of THG in silicon. Even more significantly, this work represents a nearly 100-fold reduction in pump power relative to fully phase-matched THG in periodically-poled lithium niobate (PPLN)/potassium titanyl phosphate (KTP) waveguides<sup>29</sup>. Although a comparable power density ( $\sim \text{GW cm}^{-2}$ ) has been achieved in ultrahigh-Q ( $> 1 \times 10^7$ ) cavities<sup>18</sup>, the advantage of the photonic-crystal waveguide approach is that the full bandwidth of short optical pulses can be accommodated. We estimate our conversion efficiency  $\eta$  to be  $\sim 1 \times 10^{-7}$  (or  $5 \times 10^{-10}$  for 1 W of peak pump power), which represents an increase of five orders of magnitude over that reported in three-dimensional polystyrene photonic crystals ( $\eta \approx 1 \times 10^{-15}$  for 1 W peak pump power as inferred from the quoted value of  $\eta \approx 1 \times 10^{-5}$  at  $P_\omega = 10$  MW; ref. 22). This efficiency could be further improved, for example, by decreasing the effective area ( $\eta \propto 1/A_{\text{eff}}^3$ ) or the group velocity ( $\eta \propto n_g^3$ ). A group velocity of  $c/80$  can be reasonably well achieved with this photonic-crystal waveguide design<sup>24</sup>; this would provide an order of magnitude improvement in  $\eta$ . Efficiency could also be improved at high pump powers by reducing nonlinear losses (in particular due to free carriers) through techniques such as ion implantation.

As well as tight optical confinement and slow light, the two-dimensional photonic-crystal geometry offers additional versatility to improve the efficiency of the generation and extraction of third-harmonic light. In periodic structures, the phase-matching condition,  $\Delta k = 0$ , is relaxed to  $\Delta k = \pm mG$ , where  $mG$  can be any reciprocal lattice wavevector, increasing the possibilities for phase matching (see Methods). Perhaps more importantly in our case, because the absorption length at  $3\omega$  is extremely short (3 dB  $\mu\text{m}^{-1}$  absorption loss at 520 nm in silicon<sup>30</sup>), the photonic crystal also provides a suitable platform for extracting light by coupling to surface radiating modes above the light line. The directive nature of the emission ( $\sim 10^\circ$ ) as well as the absence of green emission from the access waveguides, suggests that a component of the third-harmonic Bloch mode in the photonic crystal lies above the light line, as illustrated by the band structure in Fig. 2a. This provides a mechanism for the THG to be extracted out of plane. However, because the  $3\omega$  Bloch mode also contains harmonic components well confined in the photonic-crystal slab below the light line, the measured picowatt level of green emission is expected to be significantly lower than the total THG power generated in the photonic-crystal waveguide. The conversion efficiency reported above is therefore a conservative estimate. In addition, the photonic-crystal waveguide geometry was not optimized for third-harmonic extraction in this study, so modification may well increase overall

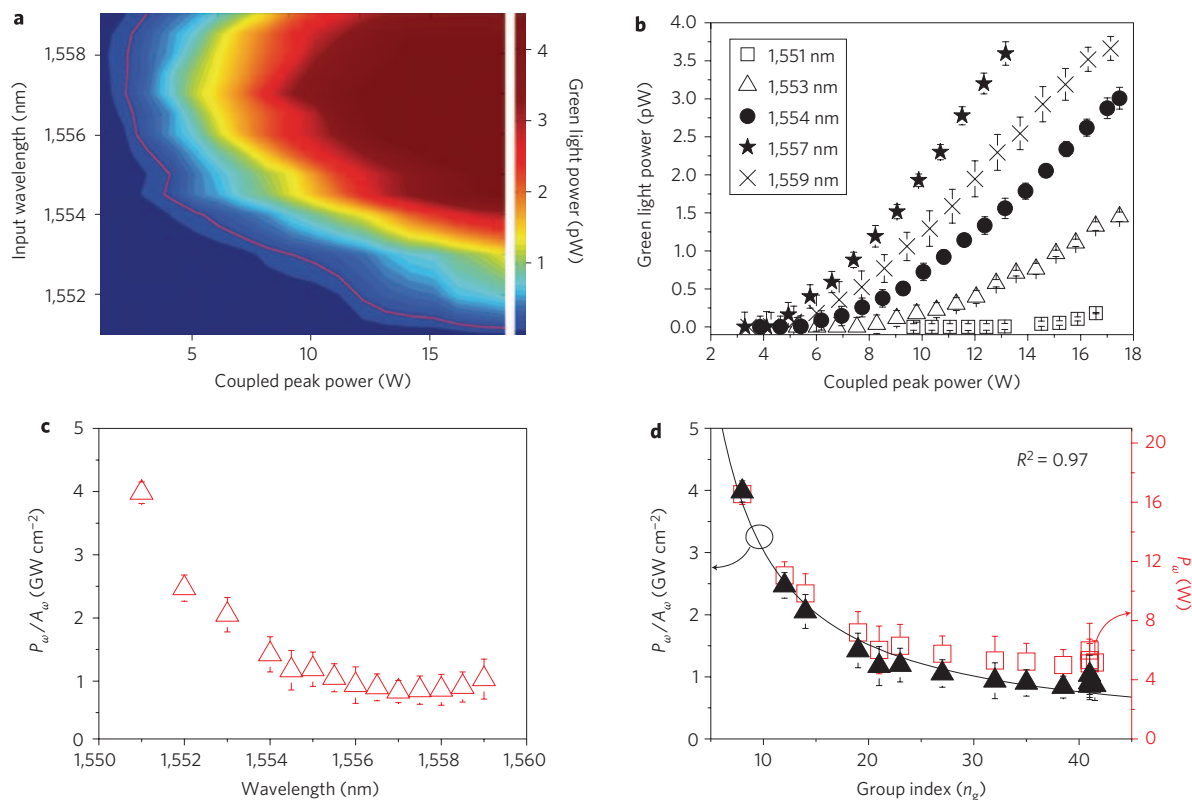


**Figure 5 | Slow-light enhancement of green light emission.** **a, b**, Green light power as a function of coupled near-infrared peak power ( $P_{\omega}$ ) for varying pump wavelengths. The constant power contour used for Fig. 5c,d appears as the dashed red line in **a**. **c, d**, Coupled peak power density ( $P_{\omega}/A_{\omega}$ ) of the pump needed to observe a constant third-harmonic power of 0.2 pW as a function of the pump wavelength (**c**) and group index  $n_g$  (**d**). The error bars are derived from noise estimation on the CCD. The solid line in **d** represents a  $1/n_g$  fit expected from the  $n_g$ -enhancement of the optical energy density.  $R^2$  is a measure of goodness-of-fit.

device efficiency. Finally, we note that the optimization of all of these processes can be done across a wide range of frequencies, allowing one to address the entire visible spectrum, or to extend the THG to other spectral windows.

In conclusion, we report optical THG of visible (green) light, enhanced by a reduction in the group velocity, or slow light in two-dimensional silicon photonic-crystal waveguides. We observe visible green emission for only  $\sim 10$  W peak pump powers due to both the tight light confinement within the photonic-crystal waveguide and the energy density enhancement provided by the slow-light mode. Following recent observations of other nonlinear effects, such as efficient Raman amplification and four-wave mixing, the THG observed here further highlights the rich photonic functionality available with the silicon photonics platform.

## Methods

**Device structure and fabrication.** The two-dimensional photonic-crystal structure consisted of a triangular lattice of air holes with lattice constant  $a = 414$  nm and hole radius 118 nm ( $0.286a$ ) etched into a 220-nm-thick silicon suspended membrane. A W1 waveguide was introduced by omitting a single row of holes along the  $\Gamma K$  direction to form a linear defect. The total photonic crystal length was 80  $\mu\text{m}$ , and the lattice period of the first and last 10 periods was increased to 444 nm parallel to the waveguide to enhance coupling to the slow-light mode<sup>31</sup>. The dispersion of the photonic-crystal waveguide was engineered by shifting the first two rows of holes adjacent to the guide perpendicular to the direction of propagation<sup>24</sup>. For the waveguide used in this experiment, the first and second rows were shifted 52 nm away from and 12 nm toward the axis of the waveguide, respectively. Light was coupled in and out of the photonic-crystal waveguide through 2-mm-long ridge access waveguides with widths tapered from 3 to 0.7  $\mu\text{m}$  over 200  $\mu\text{m}$  close to the photonic-crystal waveguide, to improve coupling to the photonic crystal. The GVD  $\beta_2$  for the engineered photonic-crystal guided mode ranged between  $3 \times 10^{-21}$  to  $2.5 \times 10^{-20}$   $\text{s}^2 \text{m}^{-1}$  for the spectral window of interest, providing an associated dispersion length for 1.5 ps pulses from 90 to 750  $\mu\text{m}$ . This is longer than the entire photonic-crystal waveguide length

and much longer than the small 5  $\mu\text{m}$  region considered in Fig. 5, and so we expect the effects of dispersion on our measurements to be negligible.

Note that this device was not optimized in terms of losses, which were dominated by coupling losses. There are several obvious routes to further improve this, for example, through the use of inverse tapers at the end-facets. The loss of 17 dB extracted from Fig. 4 comprises out-coupling losses (typically  $\sim 10$  dB and measured to be at best  $\sim 8$  dB), propagation loss in the ridge and nanowire segments ( $\sim 2$ –3 dB), scattering loss at the nanowire/photonic crystal interface ( $< 1$  dB) and the propagation losses in the photonic-crystal waveguide in the slow-light regime (2–3 dB).

The device was fabricated from a SOITEC silicon-on-insulator wafer by electron-beam lithography (hybrid ZEISS GEMINI 1530/RAITH ELPHY) and reactive ion etching using a  $\text{CHF}_3/\text{SF}_6$  gas mixture. The silica layer under the photonic-crystal slab was selectively under-etched using a HF solution to leave the photonic crystal section in a suspended silicon membrane. More details of the procedure are given in ref. 32.

**Transmission experiment.** The device was probed using a polarization-controlled, near transform-limited, figure-of-eight fibre laser, tunable over the C-band. The pulses were sech<sup>2</sup>-shaped,  $\sim 1.5$  ps long, with a spectral full-width at half-maximum of  $\sim 2$  nm, and were amplified through an erbium-doped fibre amplifier. The pulses were launched into the transverse electric (TE)-like mode of the waveguide, using lensed fibres with a 2.5- $\mu\text{m}$  focal spot diameter. To calculate the coupled power in Figs 4 and 5 from the power launched into the input lensed fibre, we estimated an in-coupling insertion loss of 8 dB. This is a typical value obtained from independent self-phase-modulation measurements on the same waveguide. Because this coupling loss is nonetheless the lowest typically measured, our estimation of the THG efficiency represents a low, or conservative, limit of the third-harmonic efficiency.

**Green light measurement.** The linearized, fixed-gain, CCD camera (Cohu 4910) was calibrated using a doubled Nd:YAG laser diode with a low relative intensity noise (RIN) with the power externally controlled by an attenuator assembly and monitored with a thermopile detector (Coherent PS10 and PowerMax meter).

**Calculations.** The band structures in Fig. 2a were calculated with a two-dimensional finite-difference time-domain (FDTD) method using effective material indices of 2.81 and 4.1 at the fundamental ( $\sim 1,550$  nm) and third-harmonic ( $\sim 520$  nm)

wavelengths, respectively, to account for the effects of confinement by the slab and the material dispersion of silicon<sup>30</sup>. Calculations were performed for a lattice period of  $a = 414$  nm and hole radius  $r = 0.286a$ , given by the experimental parameters. The calculated dispersion curves for the fundamental mode at 1,550 nm were redshifted by less than 4% relative to the experimental measurements in Fig. 2b. The band structure shows that several symmetric modes ( $H_y$ , symmetric across the waveguide, like the fundamental mode) exist at wavelengths close to 520 nm that can sustain the THG emission. We believe that the third-harmonic light is most likely coupled to the refractive-like mode highlighted by the dotted red line of Fig. 2a, which has the same symmetry as, and significant overlap with, the fundamental mode at 1,550 nm. Observation also yields an exit angle for the third-harmonic light at  $\sim 10^\circ$  from the normal, which is reasonably consistent with coupling to this mode. We observed no noticeable change in exit angle with pump wavelength over the 10-nm wavelength range near 1,560 nm studied here, leading us to believe that there is no significant change in the third-harmonic mode over this range.

The effective mode field area ( $A_{\omega}$ ) of the fundamental mode was calculated using a three-dimensional plane wave method (PWM) and the equation

$$A_{\omega} = \frac{1}{a} \cdot \frac{(\int_{\text{Vol}} |E|^2 dV)^2}{\int_{\text{Vol}} |E|^4 dV}$$

where  $E$  is the electric field amplitude of the mode and Vol is the volume of a unit cell of length  $a$  associated with the photonic-crystal waveguide. This yields an increase of  $A_{\omega}$  from 0.4 to 0.6  $\mu\text{m}^2$  for increasing wavelength over the range studied.

**Phase-matching considerations.** One might expect that because the fundamental wavevector varies by  $\sim 10\%$  as the wavelength is tuned over a 10-nm range near 1,560 nm, it may influence the wavelength variation of the THG efficiency through the phase-matching term. In order to shed some light on the conclusion of our work that the observed enhancement in THG efficiency over the wavelength range studied is solely due to the group index  $1/n_g$ , we find it useful to compare characteristic length scales in our device. In periodic structures, the phase mismatch  $\Delta k$  between the fundamental and the third-harmonic modes is defined at  $\pm mG$ , where  $mG$  can be any reciprocal lattice wavevector. Therefore,  $\Delta k < \pi/a$  (where  $a$  is the photonic-crystal lattice constant) and the associated coherence (or beating) length between the two modes  $L_{\text{coh}}$ , is thus always  $> 2a$  ( $\sim 0.83$   $\mu\text{m}$ ). From the specific band structure of Fig. 2a we further expect the coherence length to be above 2  $\mu\text{m}$ . In silicon, because the absorption length of the third-harmonic light at 520 nm is  $\sim 1$   $\mu\text{m} < L_{\text{coh}}$ , the influence of phase-matching variation on the THG efficiency in our device is expected to be negligible. Further, notwithstanding this argument or the experimental evidence, we investigated the wavelength dependence of phase matching in our device by calculating it from the band structure, based on coupling to the third-harmonic mode discussed above, and assuming no losses at the third-harmonic wavelength, and we found that it was quite different to what was observed. Hence, for all of these reasons we believe these results conclusively demonstrate direct slow-light enhancement of this nonlinear process.

Received 23 October 2008; accepted 24 February 2009;  
published online 22 March 2009

## References

- Krauss, T. F. Why do we need slow light? *Nature Photon.* **2**, 448–449 (2008).
- Baba, T. Slow light in photonic crystals. *Nature Photon.* **2**, 465–473 (2008).
- Soljacic, M. *et al.* Photonic-crystal slow-light enhancement of nonlinear phase sensitivity. *J. Opt. Soc. Am. B* **19**, 2052–2059 (2002).
- Bhat, N. A. R. & Sipe, J. E. Optical pulse propagation in nonlinear photonic crystals. *Phys. Rev. E* **64**, 0566041 (2001).
- Settle, M. D. *et al.* Flatband slow light in photonic crystals featuring spatial pulse compression and terahertz bandwidth. *Opt. Express* **15**, 219–226 (2007).
- Krauss, T. F. Slow light in photonic crystal waveguides. *J. Phys. D* **40**, 2666–2670 (2007).
- McMillan, J. E., Yang, X. D., Panoiu, N. C., Osgood, R. M. & Wong, C. W. Enhanced stimulated Raman scattering in slow-light photonic crystal waveguides. *Opt. Lett.* **31**, 1235–1237 (2006).
- Jalali, B. Teaching silicon new tricks. *Nature Photon.* **1**, 193–195 (2007).
- Vlasov, Y. A., O'Boyle, M., Hamann, H. F. & McNab, S. J. Active control of slow light on a chip with photonic crystal waveguides. *Nature* **438**, 65–69 (2005).

- Bogaerts, W. *et al.* Nanophotonic waveguides in silicon-on-insulator fabricated with CMOS technology. *J. Lightwave Technol.* **23**, 401–412 (2005).
- Lin, Q., Painter, O. J. & Agrawal, G. P. Nonlinear optical phenomena in silicon waveguides: Modeling and applications. *Opt. Express* **15**, 16604–16644 (2007).
- Jacobsen, R. S. *et al.* Strained silicon as a new electro-optic material. *Nature* **441**, 199–202 (2006).
- Wynne, J. J. Optical third-order mixing in GaAs Ge Si and InAs. *Phys. Rev.* **178**, 1295–1303 (1969).
- Wang, C. C. *et al.* Optical third harmonic generation in reflection from crystalline and amorphous samples of silicon. *Phys. Rev. Lett.* **57**, 1647–1650 (1986).
- Moss, D. J., Van Driel, H. M. & Sipe, J. E. Third harmonic generation as a structural diagnosis of ion-implanted amorphous and crystalline silicon. *Appl. Phys. Lett.* **48**, 1150–1152 (1986).
- Moss, D. J., Van Driel, H. M. & Sipe, J. E. Dispersion in the anisotropy for optical third harmonic generation in Si and Ge. *Opt. Lett.* **14**, 57–59 (1989).
- Boyd, R. *Nonlinear Optics*, Ch. 2 (Academic Press, 1992).
- Carmon, T. & Vahala, K. J. Visible continuous emission from a silica microphotonic device by third-harmonic generation. *Nature Phys.* **3**, 430–435 (2007).
- Martemyanov, M. G. *et al.* Third-harmonic generation in silicon photonic crystals and microcavities. *Phys. Rev. B* **70**, 073311 (2004).
- Dolgova, T. V., Maidikovski, A. I., Martemyanov, M. G., Fedyanin, A. A. & Aktsipetrov, O. A. Giant third-harmonic in porous silicon photonic crystals and microcavities. *JETP Lett.* **75**, 15–19 (2002).
- Coquillat, D. *et al.* Enhanced second- and third-harmonic generation and induced photoluminescence in a two-dimensional GaN photonic crystal. *Appl. Phys. Lett.* **87**, 101106 (2005).
- Markowicz, P. P. *et al.* Dramatic enhancement of third-harmonic generation in three-dimensional photonic crystals. *Phys. Rev. Lett.* **92**, 083903 (2004).
- Frandsen, L. H., Lavrinenko, A. V., Fage-Pedersen, J. & Borel, P. I. Photonic crystal waveguides with semi-slow light and tailored dispersion properties. *Opt. Express* **14**, 9444–9450 (2006).
- Li, J., White, T. P., O'Faolain, L., Gomez-Iglesias, A. & Krauss, T. F. Systematic design of flat band slow light in photonic crystal waveguides. *Opt. Express* **16**, 6227–6232 (2008).
- Kubo, S., Mori, D. & Baba, T. Low-group-velocity and low-dispersion slow light in photonic crystal waveguides. *Opt. Lett.* **32**, 2981–2983 (2007).
- Notomi, M. *et al.* Extremely large group-velocity dispersion of line-defect waveguides in photonic crystal slabs. *Phys. Rev. Lett.* **87**, 2539021 (2001).
- Engelen, R. J. P. *et al.* The effect of higher-order dispersion on slow light propagation in photonic crystal waveguides. *Opt. Express* **14**, 1658–1672 (2006).
- Gomez-Iglesias, A., O'Brien, D., O'Faolain, L., Miller, A. & Krauss, T. F. Direct measurement of the group index of photonic crystal waveguides via Fourier transform spectral interferometry. *Appl. Phys. Lett.* **90**, 261107 (2007).
- Rusu, M. *et al.* Efficient generation of green and UV light in a single PP-KTP waveguide pumped by a compact all-fiber system. *Appl. Phys. Lett.* **88**, 121105 (2006).
- Green, M. A. & Keevers, M. J. Optical properties of intrinsic silicon at 300 K. *Prog. Photovoltaics Res. Appl.* **3**, 189–192 (1995).
- Hugonin, J. P., Lalanne, P., White, T. P. & Krauss, T. F. Coupling into slow-mode photonic crystal waveguides. *Opt. Lett.* **32**, 2638–2640 (2007).
- O'Faolain, L. *et al.* Low-loss propagation in photonic crystal waveguides. *Electron. Lett.* **42**, 1454–1455 (2006).

## Acknowledgements

This work was supported by the EU-FP6 Marie Curie Fellowship project SLIPPRY, the EU-FP6 Network of Excellence ePIXnet and the EU-FP6 SPLASH project. Fabrication was carried out in the framework of the ePIXnet Nanostructuring Platform for Photonic Integration. We would also like to acknowledge the Australian Research Council (ARC) through its Federation Fellow, Centre of Excellence and Discovery Grant programs as well as the International Science Linkages program of the Australian Department of Education, Science and Technology.

## Additional information

Reprints and permission information is available online at <http://npg.nature.com/reprintsandpermissions/>. Correspondence and requests for materials should be addressed to C.M.